PAPER

Small far-red cationic benzoquinone diimine dyes†

Tatiana Munteanu, [a] Carmelo Naim, [b] Gabriel Canard, [a]
Denis Jacquemin, *[b,c] Olivier Siri *[a] and Simon Pascal *[a,b]

Two compact far-red cationic benzoquinone diimine dyes were synthesized, having molecular weights lower than 400 or 300 Da and featuring light absorption properties centered around 700 nm. Their redox and optical properties were investigated experimentally, alongside theoretical studies of their structural and excited-state characteristics.

Introduction

The development of far-red and near-infrared (NIR) dyes has been a key focus over recent decades, driven by their potential in cutting-edge applications. These wavelengths are particularly significant due to their compatibility with the biological transparency window, making red-NIR dyes valuable for fluorescence and photoacoustic bioimaging, as well as therapeutic applications.[1] Additionally, since a substantial portion of solar radiation falls within this spectral range, red-NIR dyes are crucial for enhancing the efficiency of solar cells, and enabling the development of transparent panels.[2,3] However, designing red-NIR dyes is often challenging, as it typically requires large chromophores with extensive π-delocalization to achieve the low HOMO–LUMO gaps needed for long-wavelength absorption.[4–6] In the actual context of decrease in natural resources and with the aim of atom economy, reducing the size of chromophores is a pressing objective. To address this challenge, different emerging strategies focus on the design of compact red-NIR cationic dyes with low molecular weights (MW < 400 Da), such as antiaromatic systems like aminofluorenes (*e.g.*, **A+**, Fig. 1),[7–9] or coupled polymethine structures like benzoquinone imines (*e.g.*, **B+**, Fig. 1).[10,11]

The design of such small quinoidal coupled polymethines relies on the combination of two 6π-electron subunits, typically forming six-membered rings linked by two single bonds. This arrangement induces electronic coupling between the subunits, reducing the HOMO–LUMO gap and redshifting the

absorption (and possibly emission) of the resulting chromophore.[12] We have been actively investigating the synthesis of 2,5-diaminobenzoquinone diimine coupled polymethines and their structure–property relationships to understand how *N*-substituents influence their electronic characteristics.[13] Since the early 2000s, it has been recognized that protonation of these quinones to form mono- or dicationic species induces pronounced bathochromic shifts, extending absorption into the visible range.[14] For example, introducing two weakly electron-donating trimethoxyphenyl *N*-substituents, as in quinone **C** (Fig. 2), enables reaching the red domain upon protonation
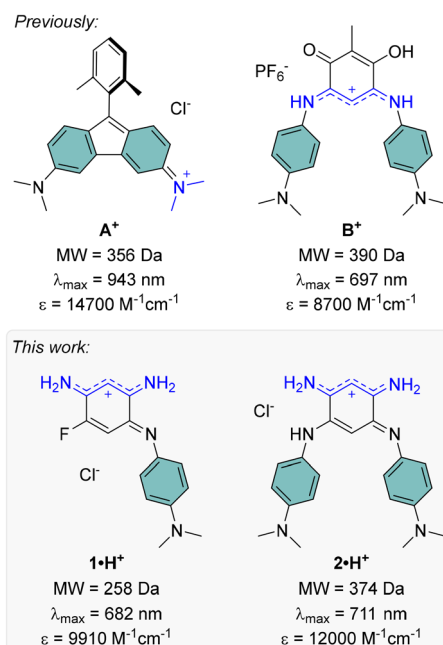

Fig. 1 Low molecular weight red-NIR cationic dyes previously reported[8,10] (top) and presented in this work (bottom), with their absorption maxima and corresponding molar extinction coefficients in solution (in water–DMSO for **A+**, in DCM for **B+**, **1·H+** and **2·H+**).

[a]Aix Marseille Univ, CNRS UMR 7325, Centre Interdisciplinaire de Nanoscience de Marseille (CINaM), Campus de Luminy, case 913, Marseille cedex 09 13288, France. E-mail: simon.pascal@cnrs.fr
[b]Nantes Université, CEISAM UMR 6230, CNRS, Nantes F-44000, France
[c]Institut Universitaire de France (IUF), Paris F-75005, France

†Electronic supplementary information (ESI) available: Additional synthetic protocols and characterizations, ^{1}H, ^{13}C and ^{19}F NMR spectra, HRMS spectra, additional electronic absorption spectra, additional theoretical data. See DOI: https://doi.org/10.1039/d5ob00082c
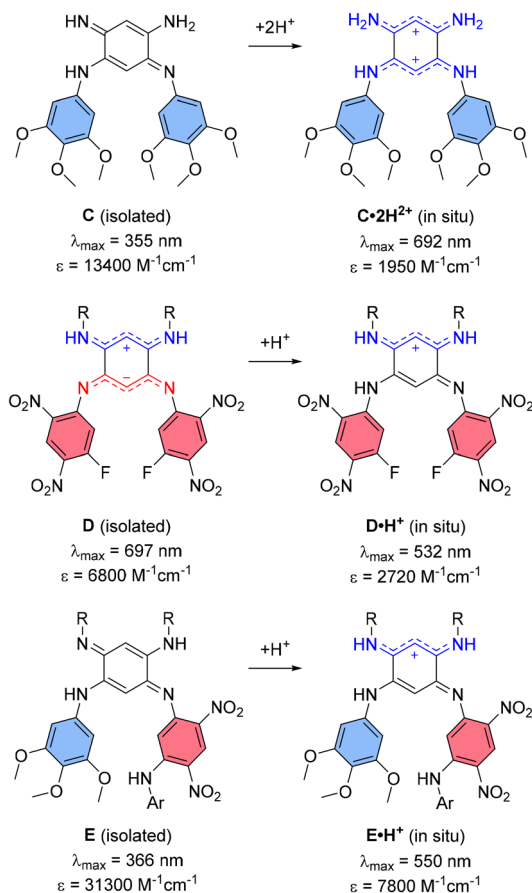
2836 | *Org. Biomol. Chem.*, 2025, **23**, 2836–2844

This journal is © The Royal Society of Chemistry 2025

Fig. 2 Previous works on diaminobenzoquinone diimines (R = C_8H_{17}; Ar = $C_6H_2(OCH_3)_3$) with their absorption maxima and corresponding molar extinction coefficients in solution (in methanol–water for **C**, in DCM for **D** and **E**).

in acidic solution.[15] Conversely, the incorporation of strongly electron-withdrawing N-substituents, as in quinone **D** (Fig. 2), stabilizes a zwitterionic ground state with a lower-energy absorption band in the red range, driven by intramolecular charge transfer (ICT); a feature however vanishing upon protonation.[16–18] In contrast, quinones bearing both types of aryl N-substituents, such as quinone **E** (Fig. 2), do not exhibit visible absorption for the neutral form and undergo noticeable red shifts upon generation of a cationic trimethine subunit in the protonated form.[19]

A notable drawback of small 2,5-diaminobenzoquinone diimines with far-red absorption is their particularly low molar extinction coefficients (ε), often attributed to nearly forbidden low-energy transitions sometimes of ICT character. While we recently succeeded in enhancing the ε of coupled heptamethine-oxonol dyes, this improvement came at the cost of significantly increasing the molecular weights of these more extended dyes, undermining efforts to maintain their compactness.[20] In the present work, we report the preparation of two new benzoquinone diimines incorporating strong electron-donating dimethylaniline substituents, **1·H⁺** and **2·H⁺**, which were isolated as stable cationic salts and exhibit strong absorp-

tion in the far-red range, while having molecular weight lower than 400 Da (Fig. 1). The optical properties and electronic structures of these compounds, along with their various protonation states, were explored through both experimental and theoretical investigations.
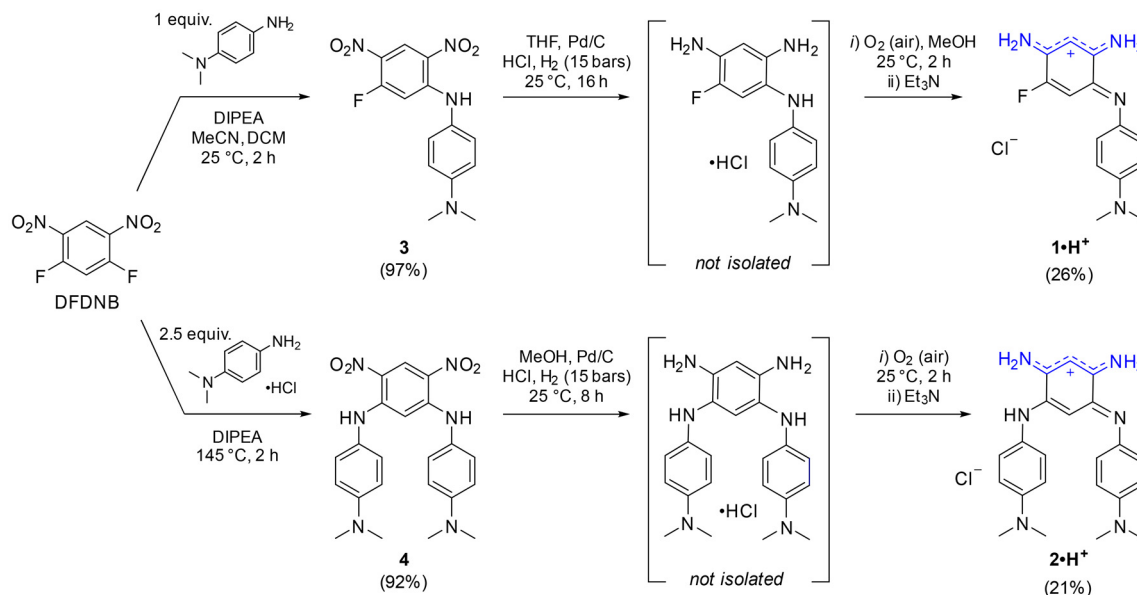
Results and discussion

Synthesis

The cationic dyes **1·H⁺** and **2·H⁺** were synthesized *via* a straightforward two-step route starting from commercially available 1,5-difluoro-2,4-dinitrobenzene (DFDNB), a highly reactive electrophile, and *N,N*-dimethyl-*p*-phenylenediamine, which acts as the nucleophile (Scheme 1). At room temperature, the reaction selectively yields the mono-substituted product **3** in 97% yield. In contrast, heating the reaction to 145 °C facilitates the substitution of both fluorine atoms in DFDNB, providing compound **4** in 92% yield.[17] The subsequent reduction of the nitro groups is performed by catalytic hydrogenation with Pd/C in acidified tetrahydrofuran or methanol. This step is immediately followed by air oxidation of the resulting aromatic tri- or tetra-amino intermediates (which are not isolated) and a basic treatment with triethylamine to neutralize the excess hydrochloric acid until the apparition of the characteristic blue coloration of the cationic dyes. The salts **1·H⁺** and **2·H⁺** were obtained as blue-purple solids in 26% and 21% yield, respectively. The striking coloration of these compounds strongly suggests their charged nature, consistent with prior observations of similar benzoquinone diimine cations. Additionally, the cationic structure of **2·H⁺** was further confirmed by performing anion metathesis with potassium hexafluorophosphate, and the ¹⁹F NMR analysis demonstrated the presence of the PF_6^- counterion (Fig. S11, ESI†).

To the best of our knowledge, aminobenzoquinone diimine structures such as **1·H⁺** have not been reported in the literature. In an effort to expand the scope of analogs of **1·H⁺**, we replaced *N,N*-dimethyl-*p*-phenylenediamine with 4-methoxyaniline. The transient blue coloration that was observed during this reaction suggested the formation of the desired product, unfortunately, it decomposed during purification (Scheme S1, ESI†). Attempts to reduce an analog of compound **3**, introducing a single *o*-phenylenediamine N-substituent, resulted in a mixture of unidentified fractions. Similarly, efforts to isolate a congener of **1·H⁺** with a hydrogen atom instead of the fluorine atom failed due to product decomposition during the purification steps. Collectively, these results highlight the critical roles played by both the strongly electron-donating *N,N*-dimethyl-*p*-phenylenediamine group and the presence of the fluorine atom at the position 5 in stabilizing and enabling the successful isolation of aminobenzoquinone diimine **1·H⁺**.

Electrochemical and photophysical properties

The electrochemical and spectroscopic properties of the isolated benzoquinone diimines were investigated experimentally

This journal is © The Royal Society of Chemistry 2025

Org. Biomol. Chem., 2025, **23**, 2836–2844 | **2837**

Scheme 1 Synthesis of benzoquinone diimines **1·H$^+$** and **2·H$^+$**.

and theoretically. Cyclic voltammetry studies provided insight into how structural modifications influence the redox behavior of the dyes (Fig. 3). Both derivatives exhibited a single irreversible one-electron reduction, occurring at −0.30 V and −0.45 V vs. Fc/Fc$^+$ for **1·H$^+$** and **2·H$^+$**, respectively. At anodic potentials, two one-electron oxidation processes were observed for each dye, with oxidation potentials at 0.89 V and 0.99 V for **1·H$^+$**, and at 0.38 V and 0.83 V for **2·H$^+$**. The shifts toward more cathodic potentials for the redox processes of **2·H$^+$** indicate its greater electron-rich nature relative to **1·H$^+$**.

The electronic absorption properties of the dyes were measured in dichloromethane (DCM) at a concentration of *ca.*

Fig. 3 Cyclic voltammograms of **1·H$^+$** (black) and **2·H$^+$** (red) recorded in *N,N*-dimethylformamide (5 × 10^{-4} M) in the presence of tetra-*n*-butylammonium hexafluorophosphate as supporting electrolyte (10^{-1} M), with a scan rate of 100 mV s^{-1}.

10^{-5} M, with the resulting spectra presented in Fig. 4 (top row) and key values compiled in Table 1. Theoretical calculations (*vide infra*) enabled the identification of the stable tautomers and isomers responsible for the observed spectra; these calculations, which also include conformational analysis and excited states computations, successfully reproduce the experimental absorption spectra, as illustrated in Fig. 4 (bottom row). Starting with the cationic species **1·H$^+$** or **2·H$^+$**, different protonation states were systematically accessed: neutral compounds were obtained by the addition of 1,8-diazabicyclo [5.4.0]undec-7-ene (DBU), while higher protonation states were achieved using trifluoroacetic acid (TFA). It is noteworthy that no emission was observed for any of the investigated species, which aligns with the non-emissive character of previously reported diaminobenzoquinone diimines.[21,22]

When dissolved in DCM, **1·H$^+$** exhibits a broad absorption band in the red region, with a maximum at 663 nm. Upon addition of DBU, the neutral species **1** is formed (Scheme 2), displaying an absorption maximum around 500 nm, which aligns well with the theoretically predicted maximum at 535 nm. Conversely, the addition of TFA induces a redshift, moving the maximum to 682 nm and increasing the molar extinction coefficient to ε^{682} = 9910 M^{-1} cm^{-1}. This suggests a complete conversion to the cationic species **1·H$^+$** (see titration, Fig. S29, ESI†). The observed peak is fitting with theoretical calculations, which predict a strongly-allowed transition redshifted to 771 nm for that species. This corresponds to an 89 nm shift from the experimental value, consistent with the expected error of the selected level of theory. However, the molar extinction coefficient is significantly overestimated in the theoretical model, calculated as ε = 44 160 M^{-1} cm^{-1}. Further addition of more than 10 equivalents of TFA causes a hypochromic shift of the red-region band and the emergence of a new transition at 454 nm with $\varepsilon \sim 2000$ M^{-1}
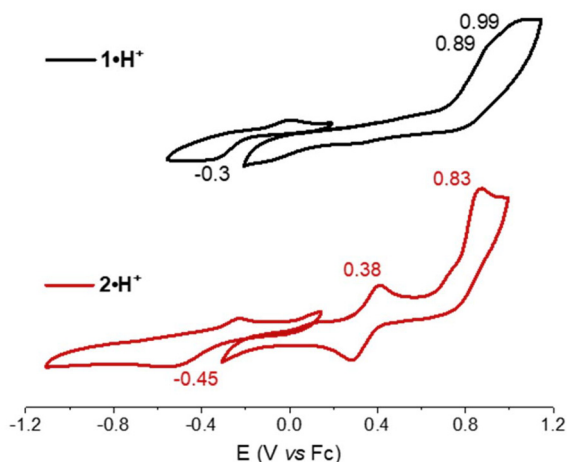
2838 | *Org. Biomol. Chem.,* 2025, **23**, 2836–2844

This journal is © The Royal Society of Chemistry 2025
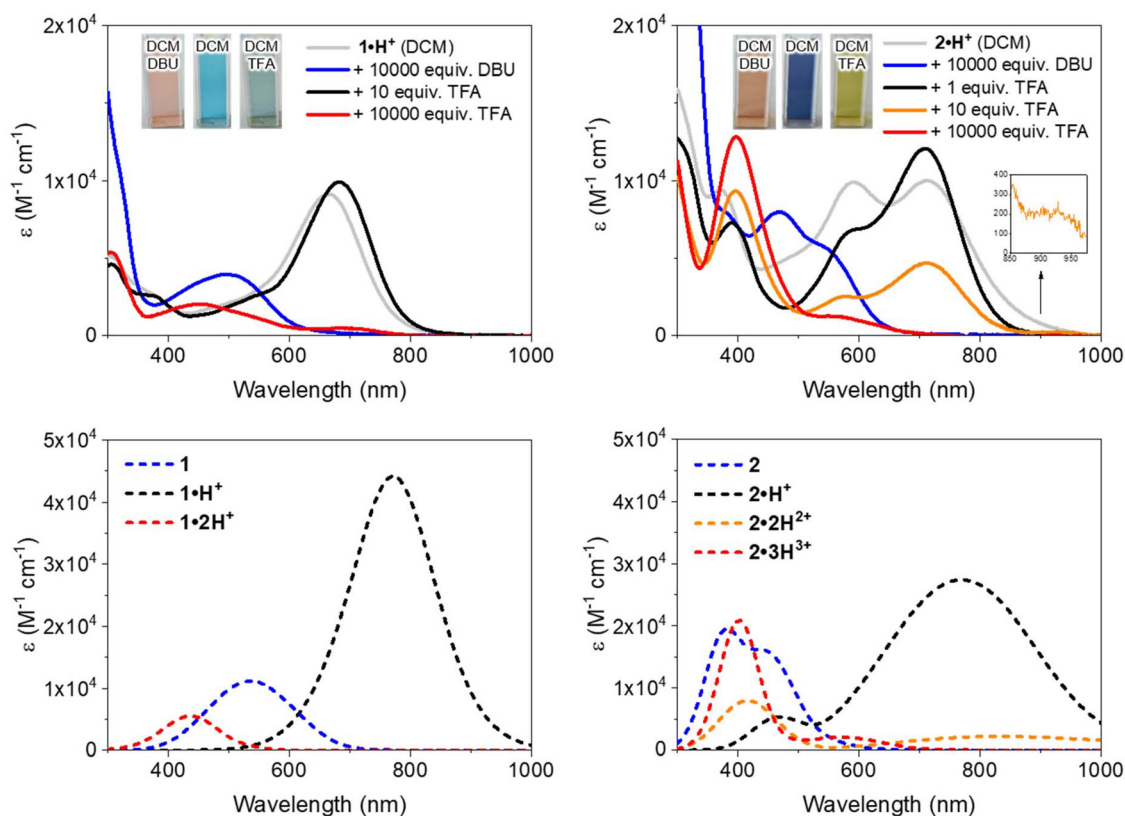
Fig. 4 Top: electronic absorption spectra of **1·H⁺** (left) and **2·H⁺** (right) in DCM (*ca.* 10⁻⁵ M) without or with the presence of DBU (1,8-diazabicyclo (5.4.0)undec-7-ene) or TFA (trifluoroacetic acid). Bottom: theoretically determined electronic absorption spectra of the protonation states of **1** (left) and **2** (right) in DCM.

Table 1 Experimental and theoretical electronic absorption bands of the different protonation states of compounds **1** and **2** in DCM

Species	Conditions in DCM	λ_{abs}^{exp} [nm] (ε^{exp} [M⁻¹ cm⁻¹])[a]	λ_{abs}^{theo} [nm] (ε^{theo} [M⁻¹ cm⁻¹])[b]
1	**1·H⁺** + 0.1 M DBU	497 (3950)	535 (11 140)
1·H⁺	**1·H⁺** + 10 equiv. TFA	682 (9910)	771 (44 160)
1·2H²⁺	**1·H⁺** + 0.1 M TFA	454 (2040)	437 (5510)
2	**2·H⁺** + 0.1 M DBU	540[c] (2780)	435 (16 210)
		471 (7970)	382 (19 570)
2·H⁺	**2·H⁺** + 1 equiv. TFA	712 (12 060)	771 (27 400)
		600[c] (6920)	470 (5340)
		390 (7290)	
2·2H²⁺	**2·H⁺** + 10 equiv. TFA	928[c] (262)	833 (2210)
		713 (4680)	415 (7970)
		578 (2550)	
		396 (9320)	
2·3H³⁺	**2·H⁺** + 0.1 M TFA	548 (1280)	569 (2060)
		397 (12 830)	402 (20 900)

[a] Absorption maxima determined in diluted DCM solution (10⁻⁵ M). [b] Theoretical data extracted from Fig. 4. [c] Shoulder.
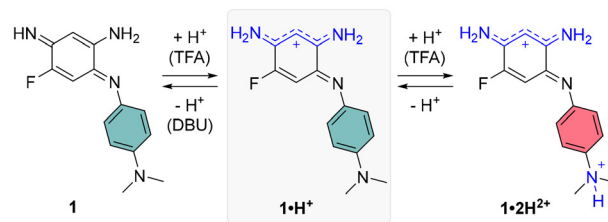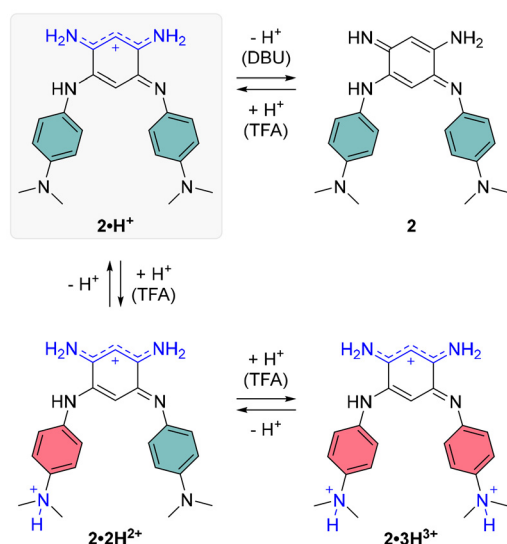

Scheme 2 Protonation states of compound **1**.

cm⁻¹, corresponding to the formation of the dicationic species **1·2H²⁺** (red spectrum, Fig. 4). This new band is well-supported by theoretical calculations, which predict an absorption at approximately 440 nm. The shift can be attributed to the protonation of

the dimethylamine group, disrupting the ICT mechanism (see below).

Regarding the symmetrical compound **2·H⁺** in DCM, it presents a broad absorption spectrum with two main bands centered around 700 and 600 nm, which appear to originate from a mixture of the neutral and mono-protonated forms, **2** and **2·H⁺** (see grey spectrum in Fig. 4). Indeed, the theoretical absorption of **2·H⁺** predicts a lower-energy transition at 771 nm, hinting that the experimental spectrum in DCM likely represents a mixture of two species. Upon addition of DBU to the solution, the absorption undergoes a significant blueshift to the 400–550 nm region (blue spectrum in Fig. 4), corresponding to the formation of the neutral quinone **2** (Scheme 3), which is also

This journal is © The Royal Society of Chemistry 2025

Org. Biomol. Chem., 2025, **23**, 2836–2844 | **2839**

Scheme 3 Protonation states of compound **2**.

predicted by theory to absorb in this range. This absorption range is consistent with those of similar electron-rich quinones bearing aniline groups, such as indamine.[23] To achieve full conversion to the cationic species **2·H⁺**, an acidic titration was performed (Fig. S30, ESI†), which revealed that upon adding one equivalent of TFA, the mixture of **2** and **2·H⁺** is fully converted to the mono-cationic species **2·H⁺**. This species is characterized by an absorption maximum centered at 712 nm with a high ε of 12 000 M^{-1} cm^{-1} (black spectrum, Fig. 4). The absorption signature of the mono-protonated form again fits the theoretically calculated values, although the experimental absorption is slightly shifted to a higher energy (711 nm *vs.* 770 nm).

The addition of ten equivalents of TFA results in a noticeable hypochromic shift in the far-red absorption band, attributed to the second protonation of the compound, progressively forming the di-cationic species **2·2H²⁺** (orange spectrum, Fig. 4). The experimental spectrum reveals a new band at 396 nm and a very weak transition in the NIR (800–1000 nm) with $\varepsilon^{928} = 262$ M^{-1} cm^{-1}, corresponding to a strong ICT from the non-protonated dimethylamine towards the core of the dye. With a large excess of TFA (10 000 equivalents), protonation of the second dimethylamine moiety diminishes the electron-donating effects of the aryl substituents, resulting in a blueshifted absorption maximum at *ca.* 400 nm, with a shoulder around 550 nm.

The absorption solvatochromism of **1·H⁺** and **2·H⁺** recorded in various solvents (Fig. S31, ESI†) reveals that the spectral variations primarily arise from the coexistence of protonated and neutral dye species in solution. Notably, slightly basic solvents (such as DMF or DMSO) favor deprotonation, increasing the proportion of neutral dyes, whereas acidic (*e.g.*, DCM) or protic solvents (*e.g.*, MeOH, H_2O) stabilize the cationic forms.

Theoretical analysis

To gain deeper insights into the structure–property relationships for the two chromophores and their various protonation states, we studied their ground-state geometries and low-lying excited states using (TD-)DFT calculations. In the neutral species **1**, conformational analysis of the tautomers reveals that the most stable geometry exhibits distinct structures for the two nitrogen atoms in the unsubstituted trimethine chain: one adopts an amine-like configuration, while the other forms an imine group (see Scheme 2 and Table S1, ESI†). This asymmetry imparts a quinone-like character to the aromatic ring. Upon protonation to form the cationic species **1·H⁺**, the
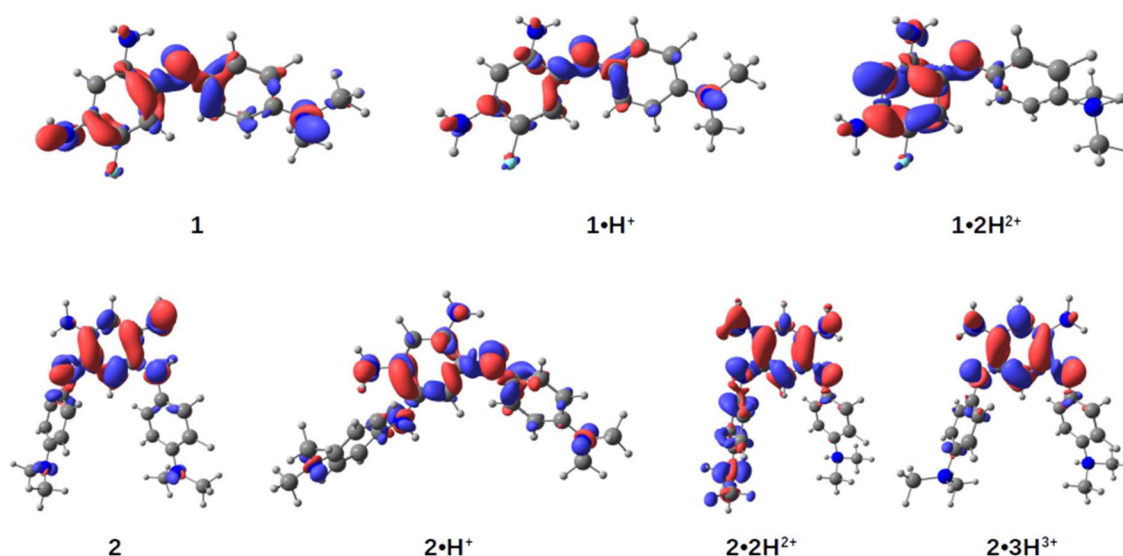
Fig. 5 Electronic density differences (EDD) between the ground (S_0) and the first excited state (S_1) for molecules **1**, **2** (most stable isomers) and their corresponding cationic forms. Regions in red indicate an increase in electronic density from S_0 to S_1, while regions in blue indicate a decrease. The isosurfaces are visualized with an isovalue of 0.003.

2840 | *Org. Biomol. Chem.*, 2025, **23**, 2836–2844

This journal is © The Royal Society of Chemistry 2025

proton preferentially binds to the imine group, localizing the positive charge on the upper trimethine subunit and stabilizing the overall structure. For the dicationic species $\mathbf{1 \cdot 2H^{2+}}$, the second proton attaches to the dimethylamino group, suppressing its electron-donating character and leaving the aromatic ring largely unchanged. Excited-state calculations attribute the observed absorption bands (Fig. 4, upper left) primarily to HOMO → LUMO transitions, characterized by high oscillator strengths (see Tables S3 and S4, ESI†). The electron density difference maps between the S_0 and S_1 states (EDD1) for $\mathbf{1}$, $\mathbf{1 \cdot H^+}$, and $\mathbf{1 \cdot 2H^{2+}}$ further elucidate the nature of these transitions (Fig. 5). In both $\mathbf{1}$ and $\mathbf{1 \cdot H^+}$, EDD1 indicates significant ICT across the molecule, with this effect being more pronounced in the neutral species. Conversely, in $\mathbf{1 \cdot 2H^{2+}}$, excitation is localized within the two trimethine subunits, consistent with the diminished electron-donating character of the protonated dimethylamino group.

For the neutral compound $\mathbf{2}$, tautomer and conformer analyses indicate that the canonical quinone structure is the most stable form, characterized by an almost coplanar arrangement of its branches (see ESI†). Similar to $\mathbf{1}$, the cationic form $\mathbf{2 \cdot H^+}$ exhibits charge delocalization along the unsubstituted trimethine chain. Protonation in $\mathbf{2 \cdot H^+}$ occurs at one of the nitrogen atoms within the unsubstituted trimethine chain (Scheme 3), resulting in two distinct isomers with a minimal free energy difference of less than 0.6 kcal mol^{-1} at room temperature (see Table S2, ESI†). The most stable isomer adopts a twisted conformation, with one branch oriented approximately 120° out of the molecular plane, whereas the less stable isomer retains coplanarity between both branches. Further protonation states, $\mathbf{2 \cdot 2H^{2+}}$ and $\mathbf{2 \cdot 3H^{3+}}$, predominantly involve the sequential protonation of the two dimethylamino groups rather than the second trimethine subunit.

Regarding excited-state calculations, the absorption spectra of $\mathbf{2}$ and its protonated forms (Fig. 4) arise from contributions of the first lowest three excited states. In the neutral compound $\mathbf{2}$, which adopts a quinone structure, the S_1 band is situated closer to other transitions in the 350–450 nm range, all exhibiting relatively low oscillator strengths. For $\mathbf{2}$, the EDD1 is predominantly localized on the core of the dye, with only minor contributions from the dimethylaniline moieties. A gain in electron density is observed at the single bonds within the core ring, which aligns with findings from related compounds previously studied by some of us.[15]

In the monocation $\mathbf{2 \cdot H^+}$, the strong NIR absorption originates from the S_1 state, dominated by a HOMO → LUMO transition with high oscillator strength (see Table S3, ESI†). Protonation of the nitrogen atom in the upper ring induces a pronounced charge-transfer character, leading to delocalization of the EDD1 across the entire molecule. We highlight that the experimental spectra likely represent a mixture of both isomers; however, as the spectral differences between these two conformers are not significant (see Fig. S34, ESI†), only the most stable isomer is reported here.

For the dication $\mathbf{2 \cdot 2H^{2+}}$, protonation of one dimethylamino group restricts delocalization to the remaining moieties of the molecule. In the trication $\mathbf{2 \cdot 3H^{3+}}$, where both dimethylamino groups are protonated, the excited state becomes confined to the core ring. In these protonation states, the S_1 band is well-separated but exhibits a reduced molar absorption coefficient. In contrast, the intense maxima in their spectra arise from the S_2 and S_3 states, which involve transitions such as HOMO−1 → LUMO and HOMO−2 → LUMO, respectively (see Table S3, ESI†).

Conclusions

In summary, we have synthesized and characterized two novel small cationic benzoquinone diimine dyes, $\mathbf{1 \cdot H^+}$ and $\mathbf{2 \cdot H^+}$, which demonstrate strong absorption in the far-red region. Through a combination of experimental studies and theoretical calculations, we established how structural modifications, protonation states, and electronic properties influence their optical behavior. Notably, the dyes exhibit higher molar extinction coefficients compared to previously reported small coupled polymethines based on quinoidal structures. These findings provide valuable insights into the design of compact red-to-NIR dyes, paving the way for further exploration of small and efficient chromophores for applications in bioimaging and optoelectronics.

Experimental section

General remarks and analysis conditions

Reagents. All reagents and solvents were purchased from Merck and were used as received. When heating was required, oil baths were used. Column chromatography was performed on silica gel 60 (230–400 mesh) or alumina 90 neutral (63–200 μm, Brockmann activity I). Analytical thin layer chromatography (TLC) was performed on precoated silica gel-60 F254 (0.5 mm) aluminium plate or precoated Al$_2$O$_3$ gel-60 neutral (0.2 mm) aluminium plate. Visualization of the spots on TLC plates was achieved by exposure to UV light. Filter aid was performed using Celite AW standard Supercel or Celite type 545. Unless otherwise specified, the desired products were dried under vacuum (<10 mbar) over 5 h at room temperature. Optical properties were recorded in spectroscopic grade solvents and employing Reagent or ReagentPlus grade 1,8-diazabicyclo(5.4.0)undec-7-ene (DBU) and trifluoroacetic acid (TFA). Compound **4** (*i.e.*, $N^1,N^{1'}$-(4,6-dinitro-1,3-phenylene)bis(N^4,N^4-dimethylbenzene-1,4-diamine)) was synthesized according to a previously reported protocol.[17]

Analytical methods and apparatus. ^{1}H, ^{13}C and ^{19}F nuclear magnetic resonance (NMR) spectra were recorded on a JEOL ECS400 NMR spectrometer at room temperature. NMR chemical shifts are given in ppm (δ) relative to Me$_4$Si using solvent residual peaks as internal standards (CDCl$_3$: δ = 7.26 ppm for ^{1}H and 77.2 for ^{13}C; DMSO-d_6: δ = 2.50 ppm for ^{1}H and 39.5 for ^{13}C; CD$_3$OD: δ = 3.31 ppm for ^{1}H and 49.1 for ^{13}C). The multiplicity of signals is designated by the following abbreviations: s, singlet; br s, broad singlet; d, doublet; br d, broad

This journal is © The Royal Society of Chemistry 2025

Org. Biomol. Chem., 2025, **23**, 2836–2844 | **2841**

doublet; t, triplet; m, multiplet. Coupling constants, J, are reported in Hertz (Hz). High resolution mass spectrometry (HRMS-ESI) analyses were performed on a QStar Elite (Applied Biosystems SCIEX) spectrometer or on a SYNAPT G2 HDMS (Waters) spectrometer by the *Spectropole* of Aix-Marseille University. These two instruments are equipped with an electrospray ionization (ESI) or a MALDI source and a TOF analyzer. Emission properties were investigated using a Horiba-Jobin Yvon Fluorolog-3 spectrofluorimeter equipped with a 450 W xenon continuous wave lamp, a three-slit double-grating excitation and a spectrograph emission monochromator with dispersions of 2.1 nm mm^{-1} (1200 grooves per mm).

Electrochemistry. Cyclic voltammetry (CV) data were recorded using a BAS 100 (Bioanalytical Systems) potentiostat and the BAS100W software (v2.3). All the experiments were conducted in a standard one-compartment using a three electrodes setup: a Pt working electrode ($\varnothing$ = 1.6 mm), a Pt counter electrode and an Ag/AgCl reference electrode (filled with a 3 M NaCl solution). Tetra-n-butylammonium hexafluorophosphate ([TBA][PF$_6$]) was used as supporting electrolyte (10^{-1} M), with a concentration of the electro-active compound of *ca.* 5×10^{-4} M. The reference electrode was calibrated using ferrocene (E°(Fc/Fc$^+$) = 0.46 V *vs.* SCE).[24] The scan rate was 100 mV s^{-1}. The solution was degassed using argon before recording each reductive scan, and the working electrode (Pt) was polished before each scan recording.

Computational details. DFT and TD-DFT calculations were performed using the Gaussian 16 package.[25] Geometry optimizations for ground-state structures and vertical excitation energies were carried out using the M06-2X exchange–correlation functional.[26] A preliminary conformational analysis was conducted with the 6-31G(d) atomic basis set to identify the most stable isomers and tautomers. Conformers with Gibbs free energy differences smaller than 2 kcal mol^{-1} relative to the most stable structure were deemed relevant and considered for further study. For these selected geometries, geometry optimization and frequency calculations were refined using the 6-311G(d,p) atomic basis set. Frequency calculations confirmed that the optimized geometries correspond to true minima of the potential energy surfaces. Excitation energies and oscillator strengths were computed using the more extensive 6-311+G(2d,p) basis set. Default protocols were employed, yet certain parameters have been tightened to enhance precision. The SCF convergence criterion was set to 10^{-10} a.u., and the "tight" option was applied for geometry optimization. Energy integrals were computed using the *superfine* integration grid, and derivatives were evaluated with the *ultrafine* grid. Solvent effects were incorporated using the implicit PCM model[27] with dichloromethane as the solvent. Geometry optimizations used equilibrium solvation parameters, while vertical absorption spectra were computed within the cLR^2 protocol,[28] accounting for both state-specific and linear response solvent effects. Transition energies were determined in the non-equilibrium solvation limit. The electronic density difference plots (EDD) have been computed as the difference between the ground- and the target excited-state electronic densities, and represented with the chemcraft code.[29]

To improve the accuracy of vertical excitation energies, CC2 corrections[30] were applied to the gas-phase TD-DFT results. Such corrections consist in shifting the TD-DFT values computed in solution (with cLR^2) using the difference between CC2 and TD-DFT values in the gas phase. CC2 calculations employed the aug-cc-pVDZ with the associated auxiliary (RI) basis set[31] and were performed using the Turbomole software applying the frozen-core approximation.[32]

Vibronic calculations were performed with the FCClasses 3 software[33] using the Vertical Hessian (VH) model within the time-dependent (TD) formalism.[34] The Franck–Condon approximation was applied for dipole expansion, *i.e.*, Herzberg–Teller effects were neglected. Geometries, gradients, and Hessians were calculated with the (TD-)DFT level described above, with transition energies refined using the cLR^2 combined with CC2 protocol. Internal coordinates were employed. To ensure easy comparisons with experimental observations, the absorption spectra were convoluted with a Gaussian broadening of 0.10 eV. For compound **1** and relative cations, absorption spectra included the first excited state, while for compound **2** and relative cations, the first three excited states were considered.

Synthetic protocols and characterizations

Synthesis of compound 3. 1,5-Difluoro-2,4-dinitrobenzene (410 mg, 2 mmol, 1 equiv.) was dissolved in a mixture of 20 mL acetonitrile and 6 mL of dichloromethane and to the solution were added N,N-dimethyl-p-phenylenediamine dihydrochloride (418 mg, 2 mmol, 1 equiv.) and N,N-diisopropyl-ethylamine (1.74 mL, 10 mmol, 5 equiv.). The reaction was stirred at room temperature and monitored by TLC, until there were no more traces of starting material (after 2 h). Then, the mixture was taken in 180 mL of dichloromethane, washed by 500 mL of water and extracted with another 20–40 mL of dichloromethane. The combined organic layers were collected, dried over anhydrous Na$_2$SO$_4$, filtered and the solvent was evaporated. The crude product was purified by column chromatography on silica gel using dichloromethane as eluent to afford **3** as a dark reddish solid (97% yield, 625 mg, 1.94 mmol). R_f: 0.7 (SiO$_2$, dichloromethane). ^{1}H NMR (CDCl$_3$, 400 MHz): δ = 9.82 (br s, 1H, NH), 9.17 (d, $^4J_{H–F}$ = 7.7 Hz, 1H, CH), 7.12 (d, ^3J = 8.2 Hz, 2H, CH), 6.78 (d, ^3J = 8.6 Hz, 2H, CH), 6.71 (d, $^3J_{H–F}$ = 13.7 Hz, 1H, CH), 3.02 (s, 6H, CH$_3$). ^{13}C NMR (CDCl$_3$, 101 MHz): δ = 161.1 (d, $^1J_{C–F}$ = 269.0 Hz, C), 150.2 (C), 149.7 (d, $^2J_{C–F}$ = 13.3 Hz, C), 128 (CH), 127.4 (C), 127.1 (CH), 126.6 (C), 125.1 (C), 124.3 (C), 113.2 (CH), 103.3 (d, $^2J_{C–F}$ = 28.8 Hz, CH), 40.5 (CH$_3$). ^{19}F (CDCl$_3$, 376 MHz): δ = −105.3. HRMS (ESI+) calculated for [M + H]$^+$: 321.0994 (C$_{14}$H$_{14}$FN$_4$O$_4^+$), found: 321.0992.

Synthesis of compound 1·H$^+$. A solution of compound **3** (200 mg, 0.62 mmol, 1 equiv.) in tetrahydrofuran (60 mL) was hydrogenated (15 bars of H$_2$) in the presence of Pd/C (5 wt%, 0.03 mmol, 66 mg) and aqueous HCl (12 M, 0.6 mL) for 16 h. Then, the mixture was stirred under air for 2 h. Methanol (*ca.* 10 mL) was added to help solubilizing the product, then triethylamine was added dropwise until a deep blue coloration of

2842 | *Org. Biomol. Chem.*, 2025, **23**, 2836–2844

This journal is © The Royal Society of Chemistry 2025

the solution was observed. Pd/C was removed by filtration through a Celite plug. The blue solution was collected, the solvent was evaporated and the crude product was purified twice over alumina oxide chromatography using dichloromethane/methanol (gradient from 9:1 to 85:15) as eluent and the product was finally precipitated in diethyl ether to afford **1·H⁺** as a blue-violet solid (26% yield, 48 mg, 0.16 mmol). R_f: 0.5 (Al_2O_3, dichloromethane/methanol, 9:1). ^{1}H NMR (CD_3OD, 400 MHz): δ = 7.31 (d, ^3J = 8.6 Hz, 2H, CH), 7.01 (d, $^3J_{H-F}$ = 12.4 Hz, 1H, CH), 6.91 (d, ^3J = 8.91 Hz, 2H, CH), 6.09 (d, $^4J_{H-F}$ = 8.5 Hz, 1H, CH), 3.18 (s, 6H, CH_3). ^{13}C NMR (CD_3OD, 101 MHz): δ = 159.5 (d, $^1J_{C-F}$ = 163.1 Hz, C), 156.1 (d, $^2J_{C-F}$ = 19.3 Hz, C), 155.2 (CH), 154.0 (C), 141.5 (d, $^2J_{C-F}$ = 5.7 Hz, C), 139.0 (C), 130.1 (CH), 114.1 (CH), 107.5 (d, $^2J_{C-F}$ = 17.7 Hz, CH), 92.5 (CH), 40.5 (CH_3). ^{19}F (CD_3OD, 376 MHz): δ = −127.19. HRMS (ESI+) calculated for (C⁺): 259.1354 ($C_{14}H_{16}FN_4^+$), found: 259.1357.

Synthesis of compound 2·H⁺. A solution of compound 4 (200 mg, 0.46 mmol, 1 equiv.) in methanol (60 mL) was hydrogenated (15 bars of H_2) in the presence of Pd/C (5 wt%, 0.02 mmol, 50 mg) and aqueous HCl (12 M, 0.4 mL) for 8 h. Then, the mixture was stirred under air for 2 h, followed by dropwise addition of triethylamine until a deep blue color of the solution was observed. Pd/C was removed by filtration through a Celite plug. The blue solution was collected, the solvent was evaporated and the crude product was purified twice over alumina oxide chromatography using dichloromethane/methanol (gradient from 95:5 to 9:1) as eluent to afford **2·H⁺** as a blue-violet solid (21% yield, 40 mg, 0.1 mmol). R_f: 0.20 (Al_2O_3, dichloromethane/methanol, 95:5). ^{1}H NMR (CD_3OD, 400 MHz): δ = 7.03 (d, ^3J = 8.7 Hz, 4H, CH), 6.75 (d, ^3J = 8.9 Hz, 4H, CH), 6.15 (s, 1H, CH), 6.00 (s, 1H, CH), 2.94 (s, 12H, CH_3). ^{1}H NMR (DMSO-d_6, 400 MHz): δ = 9.36 (br s, 2H, NH), 8.71 (br s, 3H, NH, NH_2), 7.03 (br s, 4H, CH), 6.75 (d, ^3J = 8.6 Hz, 4H, CH), 5.98 (s, 1H, CH), 5.96 (s, 1H, CH), 2.91 (s, 12H, CH_3). ^{13}C NMR did not show any signals in DMSO-d_6 and only partially resolved signals in CD_3OD due to the limited solubility of the compound. ^{13}C {DEPT135} NMR (CD_3OD, 101 MHz): δ = 125.8 (CH), 113.5 (CH), 96.8 (CH), 92.3 (CH), 40.1 (CH_3). HRMS (ESI+) calculated for (C⁺): 375.2292 ($C_{22}H_{27}N_6^+$), found: 375.2287.

Anion exchange with KPF_6

2·H⁺ was dissolved in dichloromethane and washed with an aqueous solution of KPF_6 (0.1 M), then with water. The organic layer was dried, evaporated and the product **2·H⁺ PF₆⁻** was analyzed by ^{1}H and ^{19}F NMR. ^{1}H NMR (CD_3OD, 400 MHz): δ = 6.99 (br d, ^3J = 7.6 Hz, 4H, CH), 6.72 (br d, ^3J = 6.4 Hz, 4H, CH), 6.12 (s, 1H, CH), 6.01 (s, 1H, CH), 2.91 (s, 12H, CH_3). ^{19}F NMR (CD_3OD, 376 MHz): δ = −73.78 (d, $^1J_{P-F}$ = 720 Hz).

Author contributions

Conceptualization: S. P., D. J., O. S.; investigations: T. M., S. P., G. C., C. N.; supervision: S. P., D. J., O. S.; writing – original draft: T. M., S. P., C. N., D. J.; writing – review & editing: T. M., C. N., G. C., D. J., O. S., S. P.

Data availability

The data supporting this article have been included as part of the ESI.†

Conflicts of interest

There are no conflicts to declare.

Acknowledgements

References

1 H. Li, Y. Kim, H. Jung, J. Y. Hyun and I. Shin, Near-Infrared (NIR) Fluorescence-Emitting Small Organic Molecules for Cancer Imaging and Therapy, *Chem. Soc. Rev.*, 2022, **51**, 8957–9008.

2 F. Grifoni, M. Bonomo, W. Naim, N. Barbero, T. Alnasser, I. Dzeba, M. Giordano, A. Tsaturyan, M. Urbani, T. Torres, C. Barolo and F. Sauvage, Toward Sustainable, Colorless, and Transparent Photovoltaics: State of the Art and Perspectives for the Development of Selective Near-Infrared Dye-Sensitized Solar Cells, *Adv. Energy Mater.*, 2021, **11**, 2101598.

3 D. Meng, R. Zheng, Y. Zhao, E. Zhang, L. Dou and Y. Yang, Near-Infrared Materials: The Turning Point of Organic Photovoltaics, *Adv. Mater.*, 2022, **34**, 2107330.

4 J. Fabian, H. Nakazumi and M. Matsuoka, Near-Infrared Absorbing Dyes, *Chem. Rev.*, 1992, **92**, 1197–1226.

5 G. Qian and Z. Y. Wang, Near-Infrared Organic Compounds and Emerging Applications, *Chem. – Asian J.*, 2010, **5**, 1006–1029.

6 S. Pascal, S. David, C. Andraud and O. Maury, Near-Infrared Dyes for Two-Photon Absorption in the Short-Wavelength Infrared: Strategies towards Optical Power Limiting, *Chem. Soc. Rev.*, 2021, **50**, 6613–6658.

7 A. Barker and C. C. Barker, 3:6-Disubstituted Fluorenes. Part III. Fluorene Analogues of Michler's Hydrol, Malachite-Green, and Crystal-Violet, *J. Chem. Soc.*, 1954, 1307–1309.

8 M. Grzybowski, O. Morawski, K. Nowak and P. Garbacz, Fluorene Analogues of Xanthenes – Low Molecular Weight near-Infrared Dyes, *Chem. Commun.*, 2022, **58**, 5455–5458.

9 K. Yan, Z. Hu, P. Yu, Z. He, Y. Chen, J. Chen, H. Sun, S. Wang and F. Zhang, Ultra-Photostable Small-Molecule Dyes Facilitate near-Infrared Biophotonics, *Nat. Commun.*, 2024, **15**, 2593.

10 A. Torres Ruiz, M. H. E. Bousquet, S. Pascal, G. Canard, V. Mazan, M. Elhabiri, D. Jacquemin and O. Siri, Small Panchromatic and NIR Absorbers from Quinoid Zwitterions, *Org. Lett.*, 2020, **22**, 7997–8001.

11 T. Munteanu, V. Mazan, M. Elhabiri, C. Benbouziyane, G. Canard, D. Jacquemin, O. Siri and S. Pascal, A Strategy to Design Substituted Tetraamino-Phenazine Dyes and Access to an NIR-Absorbing Benzoquinonediimine-Fused Quinoxaline, *Org. Lett.*, 2023, **25**, 3886–3891.

12 S. Dähne and D. Leupold, Coupling Principles in Organic Dyes, *Angew. Chem., Int. Ed. Engl.*, 1966, **5**, 984–993.

13 B. Mourot, D. Jacquemin, O. Siri and S. Pascal, Coupled Polymethine Dyes: Six Decades of Discoveries, *Chem. Rec.*, 2024, **24**, e202400183.

14 O. Siri, P. Braunstein, M.-M. Rohmer, M. Bénard and R. Welter, Novel "Potentially Antiaromatic", Acidichromic Quinonediimines with Tunable Delocalization of Their 6π-Electron Subunits, *J. Am. Chem. Soc.*, 2003, **125**, 13793–13803.

15 L. Lavaud, Z. Chen, M. Elhabiri, D. Jacquemin, G. Canard and O. Siri, Di- vs. Tetra-Substituted Quinonediimines: A Drastic Effect on Coordination Chemistry, *Dalton Trans.*, 2017, **46**, 12794–12803.

16 S. Pascal, L. Lavaud, C. Azarias, G. Canard, M. Giorgi, D. Jacquemin and O. Siri, Controlling the Canonical/Zwitterionic Balance through Intramolecular Proton Transfer: A Strategy for Vapochromism, *Mater. Chem. Front.*, 2018, **2**, 1618–1625.

17 S. Pascal, L. Lavaud, C. Azarias, A. Varlot, G. Canard, M. Giorgi, D. Jacquemin and O. Siri, Azacalixquinarenes: From Canonical to (Poly-)Zwitterionic Macrocycles, *J. Org. Chem.*, 2019, **84**, 1387–1397.

18 T. Horáčková, M. H. E. Bousquet, A. Morice, U. Triballier, G. Canard, P. Lhoták, D. Jacquemin, S. Pascal and O. Siri, Fully Zwitterionic Diaminobenzoquinonediimines Promoted by Cyanoaromatic N-Substituents, *Dyes Pigm.*, 2022, **206**, 110681.

19 J.-F. Longevial, Z. Chen, S. Pascal, G. Canard, D. Jacquemin and O. Siri, Stabilization of a 12-π Electrons Diamino-Benzoquinonediimine Tautomer, *Chem. Commun.*, 2021, **57**, 548–551.

20 B. Mourot, V. Mazan, M. Elhabiri, R. Sarkar, D. Jacquemin, O. Siri and S. Pascal, Insights into Extended Coupled Polymethines through the Investigation of Dual UV-to-NIR Acidochromic Switches Based on Heptamethine–Oxonol Dyes, *Chem. Sci.*, 2024, **15**, 1248–1259.

21 S. Pascal and O. Siri, Benzoquinonediimine Ligands: Synthesis, Coordination Chemistry and Properties, *Coord. Chem. Rev.*, 2017, **350**, 178–195.

22 H. Lei, S. M. Aly, P.-L. Karsenti, D. Fortin and P. D. Harvey, Luminescent Organometallic Complexes Built upon the Nonemissive Azophenine, *Organometallics*, 2017, **36**, 572–581.

23 J. F. Corbett and E. P. Gamson, Benzoquinone Imines. Part XI. Mechanism and Kinetics of the Reaction of p-Benzoquinone Di-Imines with Aniline and Its Derivatives, *J. Chem. Soc., Perkin Trans. 2*, 1972, 1531.

24 N. G. Connelly and W. E. Geiger, Chemical Redox Agents for Organometallic Chemistry, *Chem. Rev.*, 1996, **96**, 877–910.

25 M. J. Frisch, *et al.*, *Gaussian 16A.03*, Gaussian Inc., Wallingford, USA, 2016.

26 Y. Zhao and D. Truhlar, The M06 Suite of Density Functionals for Main Group Thermochemistry, Thermochemical Kinetics, Noncovalent Interactions, Excited States, and Transition Elements: Two New Functionals and Systematic Testing of Four M06-Class Functionals and 12 Other Functionals, *Theor. Chem. Acc.*, 2008, **120**, 215–241.

27 J. Tomasi, B. Mennucci and R. Cammi, Quantum Mechanical Continuum Solvation Models, *Chem. Rev.*, 2005, **105**, 2999–3094.

28 C. A. Guido, A. Chrayteh, G. Scalmani, B. Mennucci and D. Jacquemin, Simple Protocol for Capturing Both Linear-Response and State-Specific Effects in Excited-State Calculations with Continuum Solvation Models, *J. Chem. Theory Comput.*, 2021, **17**, 5155–5164.

29 Chemcraft – Graphical Software for Visualization of Quantum Chemistry Computations (version 1.8) **https://www.chemcraftprog.com**.

30 O. Christiansen, H. Koch and P. Jørgensen, The Second-Order Approximate Coupled Cluster Singles and Doubles Model CC2, *Chem. Phys. Lett.*, 1995, **243**, 409–418.

31 C. Hättig and F. Weigend, CC2 Excitation Energy Calculations on Large Molecules Using the Resolution of the Identity Approximation, *J. Chem. Phys.*, 2000, **113**, 5154–5161.

32 TURBOMOLE, V7.4.1 2019, a Development of University of Karlsruhe and Forschungszentrum Karlsruhe GmbH, 1989–2007, TURBOMOLE GmbH, since 2007. **https://www.turbomole.com**.

33 F. Santoro and J. Cerezo, FCclasses3 (version 1.0 (v3-0.1-177-g4b1514a)), 2021. **https://www.iccom.cnr.it/en/fcclasses/**.

34 F. J. Avila Ferrer, J. Cerezo, J. Soto, R. Improta and F. Santoro, First-Principle Computation of Absorption and Fluorescence Spectra in Solution Accounting for Vibronic Structure, Temperature Effects and Solvent Inhomogenous Broadening, *Comput. Theor. Chem.*, 2014, **1040–1041**, 328–337.

2844 | *Org. Biomol. Chem.*, 2025, **23**, 2836–2844

This journal is © The Royal Society of Chemistry 2025